Simulation and Modelling in Fluid Dynamics: TaskNS
Student: G. Borrelli
Prof.: E. De Angelis

1 Introduction

Purpose of the following project is to go through an analysis of the results obtained from the solution of the Navier-Stokes equations in a 2-dimensional staggered grid, following a Projection Method procedure.

The equations are here stated, in their non-dimensional form, in the case of an incompressible flow:

$$\frac{\partial u_i}{\partial x_i} = 0$$

$$\frac{\partial u_i}{\partial t} + \frac{\partial u_i u_j}{\partial x_j} = -\frac{\partial p}{\partial x_i} + \frac{1}{Re}\frac{\partial^2 u_i}{\partial x_j \partial x_j}$$

The staggered grid plays a crucial role when implementing the NSE following a Finite Differences approach. It mainly allows to preserve the coupling between velocity and pressure fields also for the largest wavenumbers, when describing the solution from the spectral point of view, exploiting a second order accurate scheme.

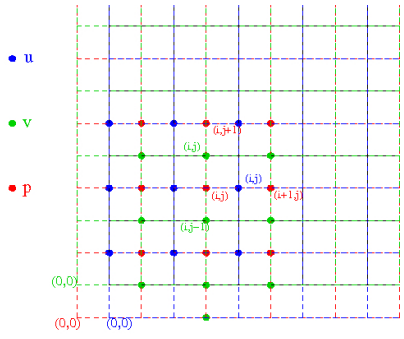

Figure 1: 2D staggered grid example.

This would not occur, instead, in the case of a classical approach, where the presence of the pressure is not 'felt' at all the wavenumbers (leading also to an increase of the errors).
In the 2D case, the staggered grid is imagined as divided into cells, with pressure (or another scalar quantity, like Φ, introduced in this method) at

the center and the velocity components (u,v) around this cell, as shown in figure 1.

The program implemented on Fortran follows the Projection Method. At first, an evaluation of a non-solenoidal solution ($\bar{w}$) is carried out.
In order to correct the latter into a divergence-free solution, a projection is required:

$$\bar{u} = \bar{w} + \nabla \Phi$$

where Φ has to be determined by solving the $\nabla^2 \Phi = -\nabla \bar{w}$ Poisson equation, in such a way that $\bar{u}$ describes the solenoidal solution of the NSE.

2 Problem Data

A channel flow is simulated, having a jet as inlet condition, with initial and boundary conditions:

- Wall-boundary condition at $y = 0$ and $y = 1$;
- Zero gradient at $x = 8$;
- Top-hat veolocity profile at $x = 0$: $u_x = 1.0$ for $0.33 < y < 0.67$ and $u_x = 0$ elsewhere.

Both Neumann and Dirichlet boundary conditions are present.

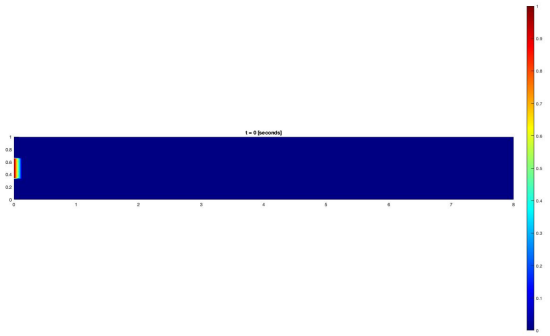

Figure 2: Initial and boundary conditions at $t = 0$ s.

The time advancement of the solution is obtained with a 2-step Runge-Kutta method, with a constraint on the time step Δt to be 0.01 (so

that 1 second will correspond to 100 iterations), and a global time evaluation of 100 seconds at least.
The solution scheme uses a spatial discretization which accounts for $Nx = 120$ points in the streamwise direction and $Ny = 48$ in the cross-stream one.
The results are analyzed at $Re = 100$ and $Re = 2000$.
Furthermore some different boundary conditions, together with different positions of the jet and resolutions of the grid, are discussed.

3 Projection method implementation

The given program had to be completed to allow for the solution of NSE in the different scenario.
First, a Finite Difference method, based on a staggered grid, has been implemented to describe the evolution in time of the two components of the velocity:

$$\frac{\partial u}{\partial t} = -\frac{\partial uu}{\partial x} - \frac{\partial uv}{\partial y} + \frac{1}{Re}\left(\frac{\partial^2 u}{\partial x^2} + \frac{\partial^2 u}{\partial y^2}\right)$$

$$\frac{\partial v}{\partial t} = -\frac{\partial uv}{\partial x} - \frac{\partial vv}{\partial y} + \frac{1}{Re}\left(\frac{\partial^2 v}{\partial x^2} + \frac{\partial^2 v}{\partial y^2}\right)$$

Which read as:

$u - component$ (j = 1,...,Ny; i = 1,...,Nx-1)

$$Rhs(I,j) = -2u(I,j)\frac{u(I+1,j)-u(I-1,j)}{2\Delta x} - u(I,j)\left(\frac{uy(ipJ)-uy(Ijm)}{\Delta y}\right) +$$

$$-\frac{uy(ipJ)+uy(Ijm)}{2}\left(\frac{u(I,j+1)-u(I,j-1)}{2\Delta y}\right) +$$

$$+\frac{1}{Re}\left(\frac{u(I+1,j)-2u(I,j)+u(I-1,j)}{\Delta x^2}\right) +$$

$$+\frac{1}{Re}\left(\frac{u(I,j+1)-2u(I,j)+u(I,j-1)}{\Delta y^2}\right)$$

$v - component$ (j = 1,...,Ny-1; i = 1,...,Nx)

$$Rhs(j,I) = -2v(i,J)\frac{v(i,J+1)-v(i,J-1)}{2\Delta y} - v(i,J)\left(\frac{ux(Ijp)-ux(imJ)}{\Delta x}\right) +$$

$$-\frac{(ux(Ijp)+ux(imJ)}{2}\left(\frac{v(i+1,J)-v(i-1,J)}{2\Delta x}\right) +$$

$$+\frac{1}{Re}\left(\frac{v(i+1,J)-2v(i,J)+v(i-1,J)}{\Delta x^2}\right)+$$
$$+\frac{1}{Re}\left(\frac{v(i,J+1)-2v(i,J)+v(i,J-1)}{\Delta y^2}\right)$$

where the expressions for $uy(ipJ), uy(Ijm), ux(Ijp)$ and $ux(imJ)$ are reported in the appendix.

Following the steps required from the Projection Method, the divergence of the non-solenoidal field has been implemented, still by means of a finite difference routine.
(At this point it is possible to assume $\bar{u} = \bar{w}$, which will then be corrected by means of the projection):

$$q(i,j) = -\left(\frac{w_x(i,j)-w_x(i-1,j)}{\Delta x}+\frac{w_y(i,j)-w_y(i,j-1)}{\Delta y}\right)$$

Finally, the first guesses for the non-solenoidal field are corrected introducing the solution Φ, obtained from the Poisson equation. The latter has been solved by a Gauss-Seidel scheme.
The projected components of the velocity read as:

$$u(I,j) = w_x(I,j) + \frac{\Phi(I+1,j)-\Phi(I,j)}{\Delta x}, \quad (j = 1, ..., Ny+1; i = 1, ..., Nx)$$

$$v(i,J) = w_y(i,J) + \frac{\Phi(i,J+1)-\Phi(i,J)}{\Delta y}, \quad (j = 1, ..., Ny; i = 1, ..., Nx+1)$$

4 Post-Processing of the Data

The post-processing has been performed in order to evaluate the main differences between solutions of the Navier-Stokes equations for different values of the Reynolds number ($Re = 100, Re = 2000$).
From a practical point of view, a difference can be appreciated already when looking at the time required to solve the problem. Indeed, in the case of Re = 100, the simulation time is of the order of some minutes, whilst when dealing with higher Re, as Re = 2000, like in this case, the amount of time may rise up to 10 hours.
This highlights the limits of simulation when moving towards higher Reynolds number. From the computational point of view, it pushes for the

implementation of schemes that will allow to reduce the complexity of the system and the amount of time required to simulate.
(In the case of a 3D simulation, this would lead to a modelling of the smallest scales of turbulence, cosequently to the cascade process).
Results are shown in figure 3 and 4:

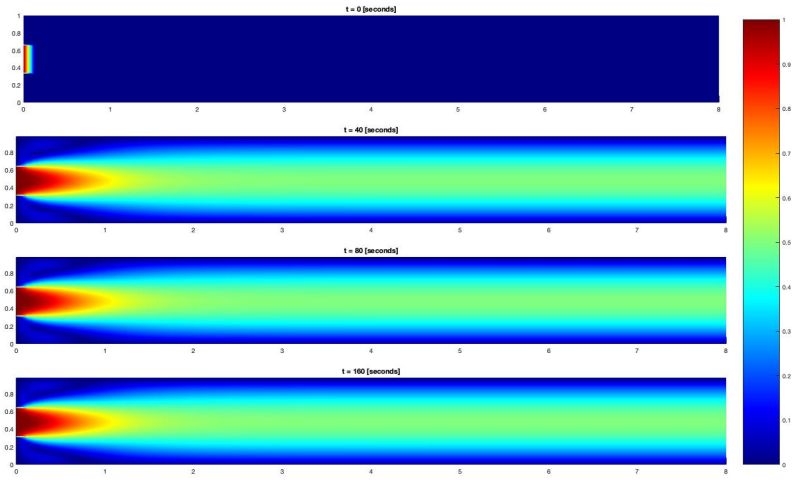

Figure 3: Velocity field for $Re = 100$.

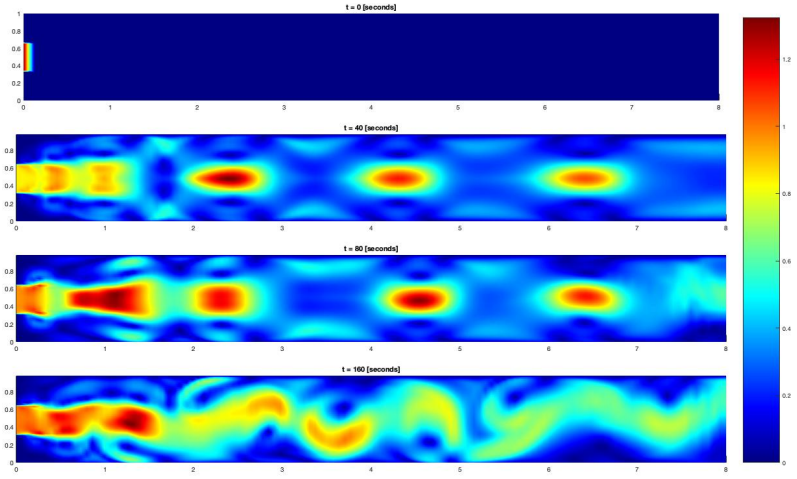

Figure 4: Velocity field for $Re = 2000$.

At a first glance, from the snapshots acquired for the two different Reynolds numbers, it is clearly visible how the velocity fields are very dissimilar.

(Re = 100)
At Re = 100, the jet has a (quasi-) steady behaviour and it reaches its fully developed configuration already after the first time instants and in the first couple of meters of the channel.
This behaviour may be observed also from the directional field for the velocities[1], in figure 5. The flow trajectories' are indeed describing a regular behaviour.

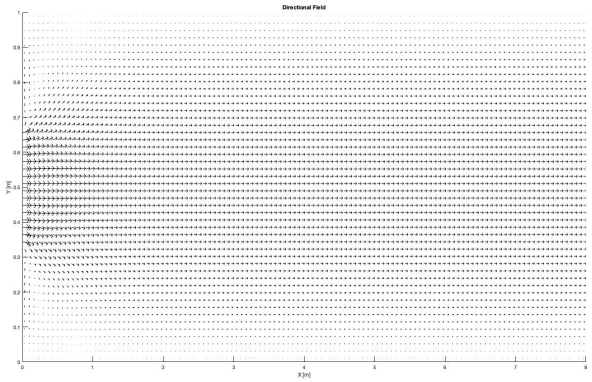

Figure 5: Directional Field at Re = 100.

The regularity may be also observed when plotting the evolution of the horizontal and vertical components of the velocities at different stations, i.e. various distances from the jet inlet.
In figure 6, the u and v components of the velocity are plotted at $x = 2.0m$ and $x = 7.0m$.
It's visible how the horizontal component preserves the intensity when moving along the channel. The profile presents a typical parabolic distribution, with the intensity being zero at the wall, due to the no-slip condition.
The vertical component is described by a smaller intensity (of the order of 10^{-3}, at $x = 2.0m$). The values below the centerline move towards the negative direction, whilst the values above move upwards, following a symmetric trend. This is consistent with the type of jet analyzed.

[1]This has been obtained by means of the Matlab built-in function 'quiver'.

Furthermore, it is interesting to notice how, when moving along the channel, the intensity of the vertical component is much reduced.
At $x = 7.0m$ the intensity has indeed become of the order of 10^{-7}. Also in this case, due to the boundary condition, the velocity at the wall is equal to zero.

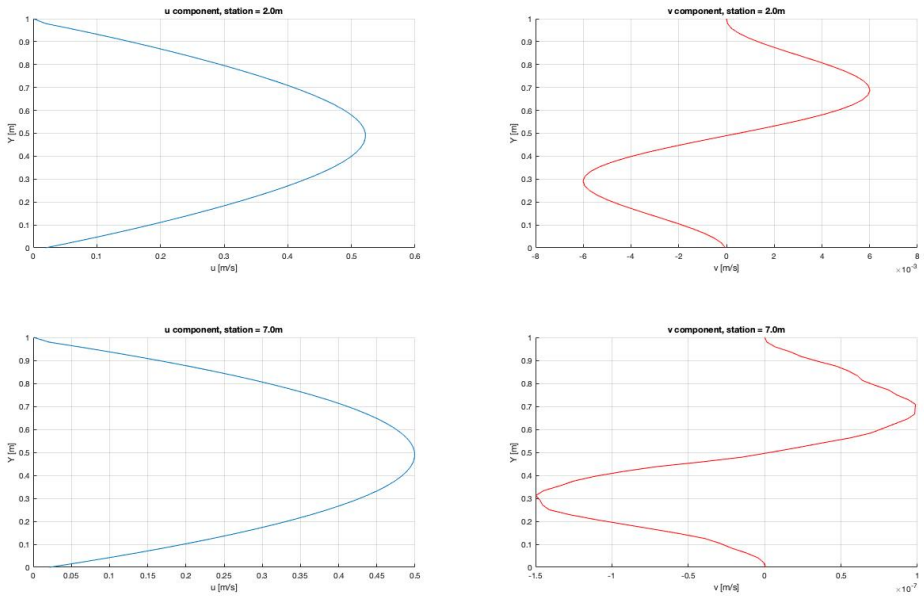

Figure 6: Span-wise distribution of the horizontal and vertical velocity components (Re = 100).

(Re = 2000)
A completely different scenario is observed in the case of Re = 2000. In figure 4, a time-dependand dynamic is easily detectable and deeply different configurations are generated for various time instants.
The red areas in the pictures indicate locations where high velocities are concentrated. This has not been observed in the case of Re = 100, where high speeds are limited only to the region around the core of the jet, due to the steadyness of the flow and to the (quickly achieved) fully developed condition.
By representing the directional field, the two-dimensional vorticity is recognizable in the concentric streamlines' patterns (see figure 7). It is useful to represent this field at different time instant also to highlight the time-dependance of the phenomenon.

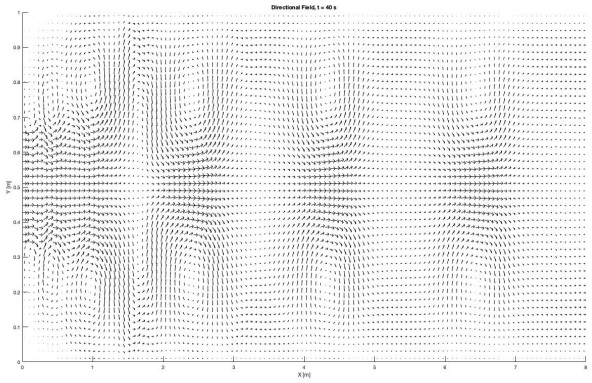

(a)

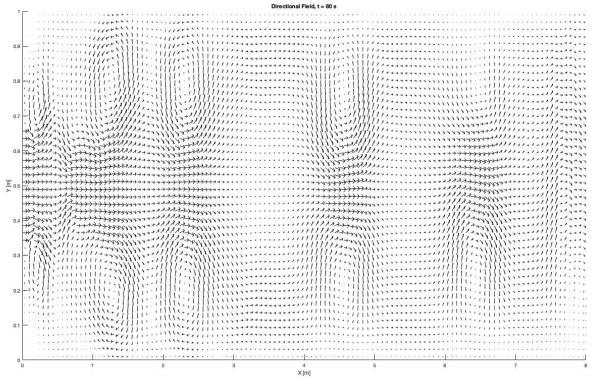

(b)

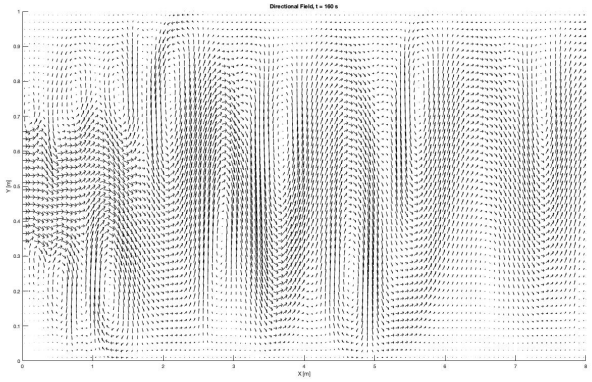

(c)

Figure 7: Directional Field at Re = 2000. (a) t=40 s, (b) t=80 s, (c) t=160 s.

Together with the time-dependance, it is useful to underline the stream-wise description of the velocity components.
By analyzing the profiles obtained at t = 160 s for $x = 2.0m$, $x = 4.0m$ and $x = 7.0m$, both components of the velocity show an irregular distribution, which may be oriented, alternatively, in both the positive and negative directions.
Another significant difference with respect to the previous case is given by the analysis of the vertical component, which, this time, maintains the same order of magnitude, in its development in the x-direction.
Still the wall-boudary conditions is respected.

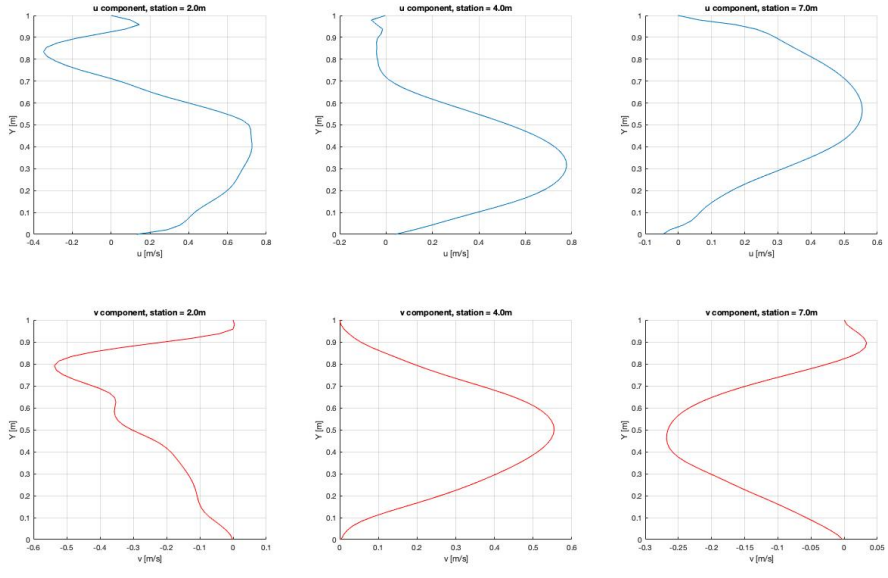

Figure 8: Span-wise distribution of the horizontal and vertical velocity components at different x-stations. (Re = 2000, t = 160 s).

5 Some Other Jet Configurations

Some more configurations have been simulated by changing the boundary conditions and the position of the jet.

(Whole inlet jet: ux = 1.0 for $0 < y < 1$)
The first alternative configuration of the jet has been achieved by extending the top-hat velocity profile to the whole span-wise length.
A big difference with the jet analyzed in the previous section is that a fully developed regime may be observed, not depending on the chosen Reynolds

number. What changes is the region represented by the highest velocities, which is wider in the case of Re = 2000, as expected.
Having the whole jet, a Boundary Layer is generated. It is cleary visible how by increasing the Reynolds number the thickess decreases, when dealing with laminar flows, as it is well-known from the theory.

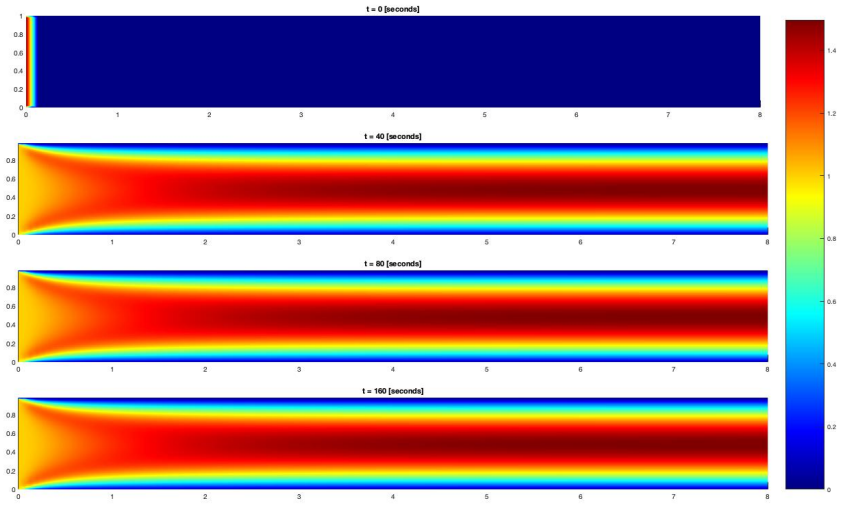

Figure 9: Velocity field of the full jet for $Re = 100$.

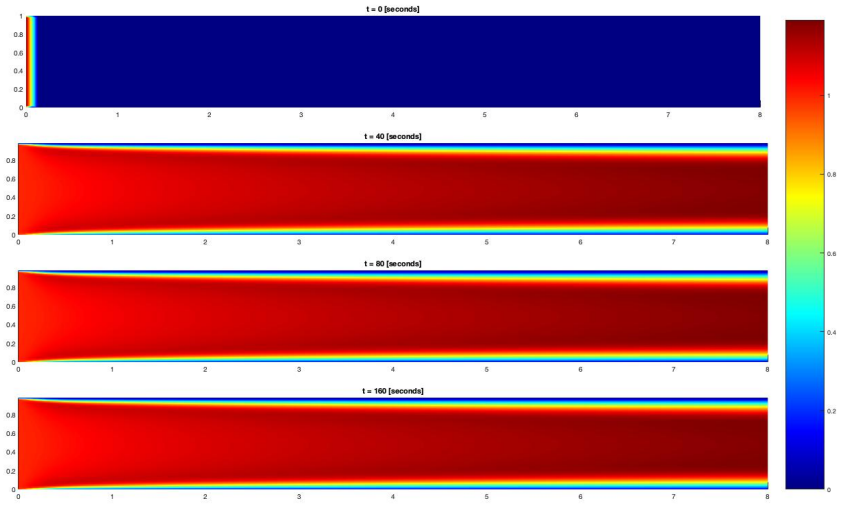

Figure 10: Velocity field of the full jet for $Re = 2000$.

The directional field is represented by a nearly homogeneous configuration, which will be described by a quasi-parallel distribution of the streamlines.

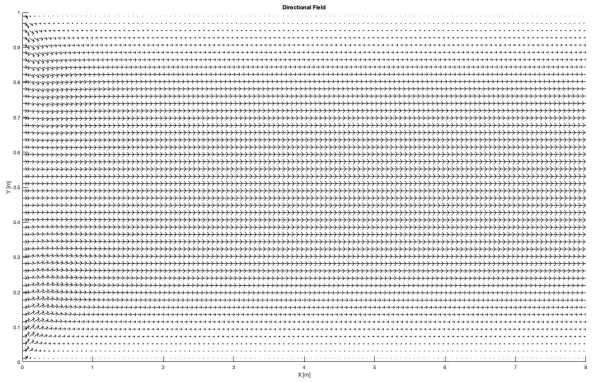

Figure 11: Directional Field for the full jet at Re = 100. (At Re = 2000 the directional field doesn't show any significant change).

Finally, the analysis of the velocity profiles related to the two components is carried out. One interesting result is shown in figure 12, where, for Re = 2000, the velocity profile in the x-direction shows a really steep gradient of the velocity in the span-wise direction.

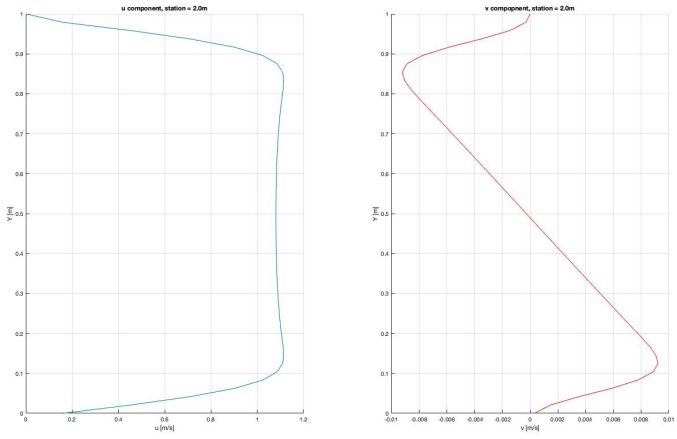

Figure 12: Span-wise distribution of the horizontal and vertical velocity components for the full-jet configuration. (Re = 2000, t = 160 s, x = 2.0m).

By recalling the definition of the skin friction, which is proportional to the gradient $\partial U/\partial y$, this result may be interpreted as an increase of the

friction with the Reynolds number.
It is important to stress the fact that in the 2D case, the variables involved are always related to a laminar solution. Turbulence does not come into play. Indeed, a necessary condition to have a turbulent flow is to have a 3D problem, which will allow to generate the cascade process leading to scale separation.

(Top jet: effect of gradual Re increase.)
Another configuration is the one of a jet coming from a small portion from the top (ux = 1.0 for $0.75 < y < 1$, see figure 13).

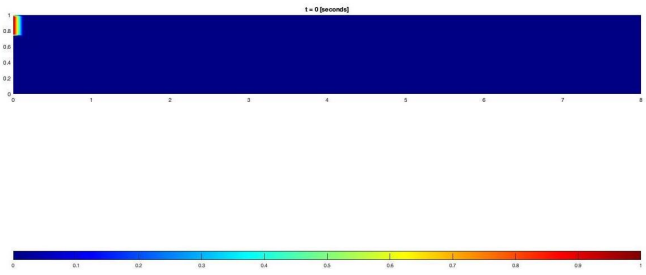

Figure 13: Velocity field of the top jet at t = 0 s.

For this case, the analysis focuses on the effect of a gradual increase of the Reynolds number in order to see how, and around which Re, the vortical motion begins to take place, starting to describe a time-dependant phenomenon.

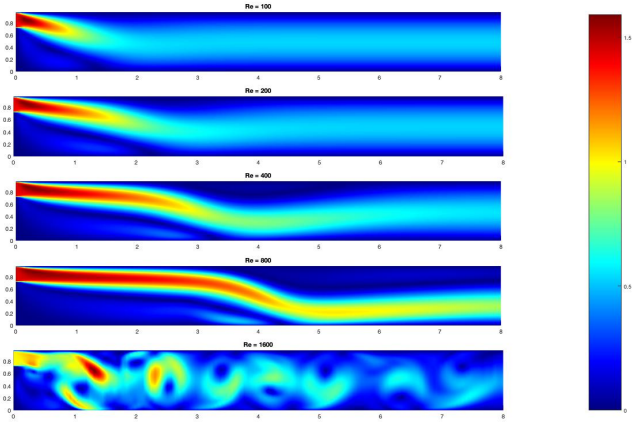

Figure 14: Velocity field of the top jet for increasing Reynolds number (t = 160s).

This is clearly observed in figure 14, where the velocity fields are compared by doubling the Re at t = 160 seconds. Initially, the figure shows how the fully developed region is moving away from the inlet as Reynolds increases. In the last two pictures this area is not seen anymore.
By observing the picture, it is also possible to conclude that a significant vorticity will be generated for Re around 1000, and that will always be more visible with the increase of it. (see also figure 4).

Having a look at the velocity profiles and the directional field in figure 15 it's clear how, initially, the vertical components of the velocity are mainly negative. Indeed, being the jet located at the top, the preferential direction of motion will be the one towards the negative y-coordinate.
Once the jet developed, the vertical velocities become smaller and mostly oriented in the positive direction of y.

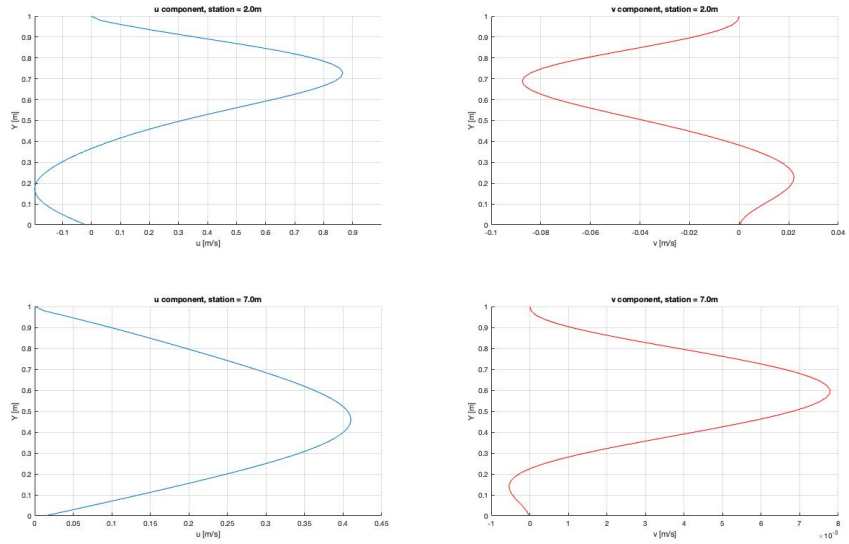

Figure 15: Velocity profiles for Re = 400 at $x = 2.0m$ and $x = 7.0m$ (t = 160s).

The horizontal components shows some negative values as well. These may be reconduced to the areas where, by increasing the Reynolds number, the vorticity will start to generate, as it is shown in figure 16.

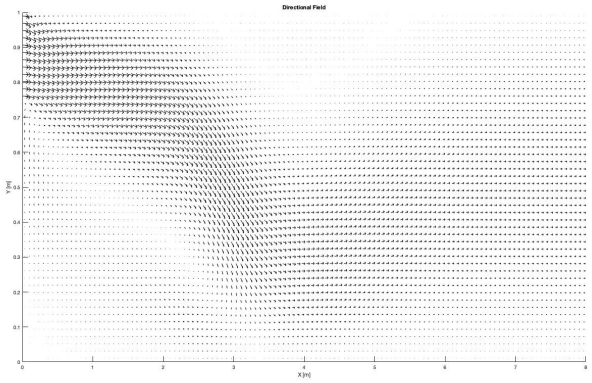

Figure 16: Directional Field of the top jet at Re = 400 (t = 160s).

(Top jet: effect of the resolution.)
One final aspect that can be investigated is the effect of the resolution. This is shown in figure 17, where still a jet coming from the top is taken into account.
The comparisons have been made at the first instants of the simulation (t = 10 s and t = 25 s) at $Re = 1600$. The low resolution simulation is carried out with a grid composed of Nx = 30 and Ny = 12 points, whilst the higher one uses the original grid of Nx = 120, Ny = 48.

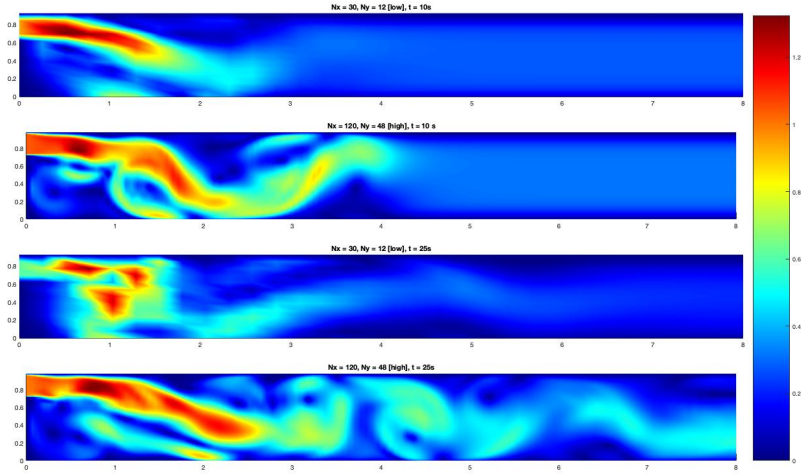

Figure 17: Velocity field compared for an high and low resolution. Re = 1600, t = 10 s and t = 25s.
High resolution: Nx = 120, Ny = 48. Low resolution: Nx = 30, Ny = 12.

It is interesting to notice how resolution affects the velocity field that is visualized. Indeed, for high Reynolds, when the phenomenon becomes time dependant and vortices are generated, the pictures that are obtained are deeply dissimilar.
The same issues have been observed also in the case of smaller Reynolds numbers. These are not reported here because they are much less significant from the visualization point of view.

Appendices

```
   uy_ipJ=.5*(Uy_k(i,J)+Uy_k(i+1,J))
   uy_Ijm=.5*(Uy_k(i,J-1)+Uy_k(i+1,J-1))

 Rhs_ux_k(I,j)=-2*Ux_k(I,j)*(0.5*un_dx)*(Ux_k(I+1,j)-Ux_k(I-1,j))-
&.5*(uy_ipJ+uy_Ijm)*(0.5*un_dy)*(Ux_k(I,j+1)-Ux_k(I,j-1))-
&Ux_k(I,j)*(uy_ipJ-uy_Ijm)*(un_dy)+
&inv_re*((Ux_k(I+1,j)-2*Ux_k(I,j)+Ux_k(I-1,j))*un_dx2)+
&inv_re*((Ux_k(I,j+1)-2*Ux_k(I,j)+Ux_k(I,j-1))*un_dy2)
```

(a)

```
   ux_Ijp=.5*(Ux_k(I,j)+Ux_k(I,j+1))
   ux_imJ=.5*(Ux_k(I-1,j)+Ux_k(I-1,j+1))

 Rhs_uy_k(i,J)=-2*Uy_k(i,J)*(0.5*un_dy)*(Uy_k(i,J+1)-Uy_k(i,J-1))-
&.5*(ux_Ijp+ux_imJ)*(0.5*un_dx)*(Uy_k(i+1,J)-Uy_k(i-1,J))-
&Uy_k(i,J)*(ux_Ijp-ux_imJ)*un_dx+
&inv_re*((Uy_k(i+1,J)-2*Uy_k(i,J)+Uy_k(i-1,J))*un_dx2)+
&inv_re*((Uy_k(i,J+1)-2*Uy_k(i,J)+Uy_k(i,J-1))*un_dy2)
```

(b)

Figure 18: FD method, together with a staggered grid, applied to the u (a) and v (b) components' evolution in time. The calculations applied to obtain $uy(ipJ), uy(Ijm), ux(Ijp)$ and $ux(imJ)$ are highlighted.

```
clear
close all
clc

% the script generates a file each 500 iterations, containing columns
% describing x,y,u,v
it_min = 0;
it_max = 16000;

% The .dat file evaluates the elements at each one of the 50 steps
% in the y-direction. For each y-steps, 122 evaluations are carried out in
% the x-direction
Lx = 8;
Nx = 122;
x = linspace(0,Lx,Nx);
x = x';
dx = Lx/(Nx-1);

Ly = 1;
Ny = 50;
y = linspace(0,Ly,Ny);
y = y';
dy = Ly/(Ny-1);

for n = 0:500:it_max
    % routine to load the data acquired each 500 iterations
    if n<1000
        xx = ['ave00',num2str(n),'.dat'];
    elseif n < 10000 && n > 1000
        xx = ['ave0',num2str(n),'.dat'];
    elseif n < 100000 && n > 10000
        xx = ['ave',num2str(n),'.dat'];
    end

    A = readtable(xx);
    A1 = table2array(A);

    u = A1(:,3);
    v = A1(:,4);

    u = reshape(u,Nx,Ny-1);
    v = reshape(v,Nx,Ny-1);

    % now calculating the modulus of the velocity given from the 2
    % components u and v
    for i = 1:Nx
        for j = 1:Ny
            vel1(i,j) = sqrt(u(i,j)^2+v(i,j)^2);
        end
    end

    figure(1)
    % plotting the velocity fields at different time instants (1 second =
    % 100 iterations, being the time step = 0.01)
    if n == 4000
        subplot(4,1,2)
        surf(y,x,vel1)
        shading interp
        colormap jet
        %colorbar
        axis equal
        caxis('auto')
```

```
        view(90,270)
        title('t = 40 [seconds]')
    end

    % if n == 8000
    %     subplot(4,1,..)
    % more subplot may be added to include the velocity field
    % representation at different time intants

    % to introduce a common colorbar in the subplot
    hp4 = get(subplot(4,1,4),'Position');
    colorbar('Position', [hp4(1)+hp4(3)+0.01  hp4(2)  0.04  hp4(2)+hp4(3)*0.9])

    if n == 16000
        % to plot the directional field, in order to visualize the
        % streamlines
        figure(2)
        axis([0,8,0,1])
        xlabel('X [m]')
        ylabel('Y [m]')
        hold on
        quiver(A1(:,1),A1(:,2),A1(:,3),A1(:,4),'k')
        title('Directional Field')

        % defining the vectors describing u and v components of the
        % fluctuations in order to compare them at a chosen spanwise
        % station (being the total length = 8, and having 120 points in the
        % x-direction, 15 points = 1 meter)

        % X = 2 meters
        u_2 = u(30,:);
        v_2 = v(30,:);
        y_span = linspace(0,1,49);

        % X = 7 meters
        u_end = u(105,:);
        v_end = v(105,:);

        figure(3)

        subplot(2,2,1)
        ylabel('Y [m]')
        xlabel('u [m/s]')
        hold on
        plot(u_2,y_span)
        title('u component, station = 2.0m')
        grid on

        % subplot(2,2,..)
        % some more subplot may be added to represent evaluations at
        % different x-positions
    end
end
```

Figure 19: General script implemented for the post processing.